

Supplementary Information

Green Preparation of High Yield Fluorescent Graphene Quantum Dots from Coal-Tar-Pitch by Mild Oxidation

Quanrun Liu ^{1,*}, Jingjie Zhang ¹, He He ¹, Guangxu Huang ^{1,2,3}, Baolin Xing ¹, Jianbo Jia ¹ and Chuanxiang Zhang ^{1,*}

¹ College of Chemistry and Chemical Engineering, Henan Polytechnic University, Jiaozuo 454003, China; zhangjingjie1221@163.com (J.Z.); hpuhehe@163.com (H.H.); guangxu1369@163.com (G.H.); baolinxing@hpu.edu.cn (B.X.); jiajianbo@hpu.edu.cn (J.J.)

² Collaborative Innovation Center of Coal Work Safety of Henan Province, Jiaozuo 454003, China

³ Henan Key Laboratory of Coal Green Conversion, Jiaozuo 454003, China

* Correspondence: qrliu@163.com (Q.L.); zcx223@hpu.edu.cn (C. Z.); Tel.: +86-10-0391-3986816 (C.Z.); Fax: +86-10-0391-3986810 (C.Z.)

Table S1. Summary of surface element content of CTP and GQDs by XPS analysis.

Sample	Elements (%)			
	C	O	N	S
CTP	93.54	3.58	2.62	0.26
GQDs-1	69.30	29.84	0.77	0.09
GQDs-2	58.85	40.10	0.98	0.07

Table S2. Summary of C chemical bonds form in the surface of CTP and GQDs.

Chemical bond type	Chemical bond proportion (%)	CTP	GQDs-1	GQDs-2
Csp^2	51.30	37.30	30.98	
Csp^3	39.49	23.59	20.35	
C-O	9.21	12.04	8.00	
C=O	-	5.86	18.28	
COOH	-	21.21	22.37	

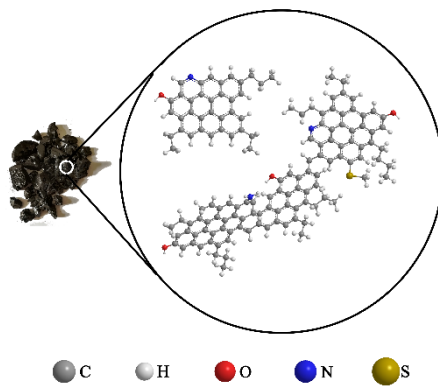


Fig. S1. Macroscale image and simplified illustrative molecular structure of CTP.

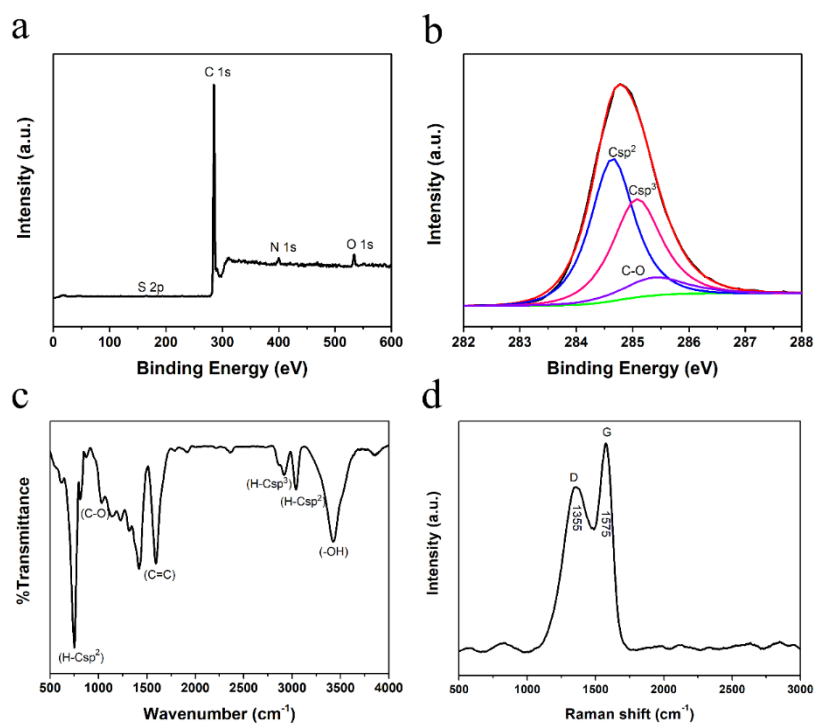


Fig. S2. Characterization of CTP. (a) XPS survey of CTP. (b) High resolution C 1s XPS spectrum of CTP displayed presence of Csp^2 , Csp^3 and C–O modes at 284.6 eV, 285.1 eV and 285.4 eV, respectively. (c) ssFTIR spectrum of CTP showing H– Csp^2 , C–O, C=C, H– Csp^3 and O–H vibration modes at 750/3040 cm^{-1} , 1032 cm^{-1} , 1593 cm^{-1} , 2917 cm^{-1} and 3426 cm^{-1} as labeled, respectively. (d) Raman spectrum of CTP under excitation of 532 nm.

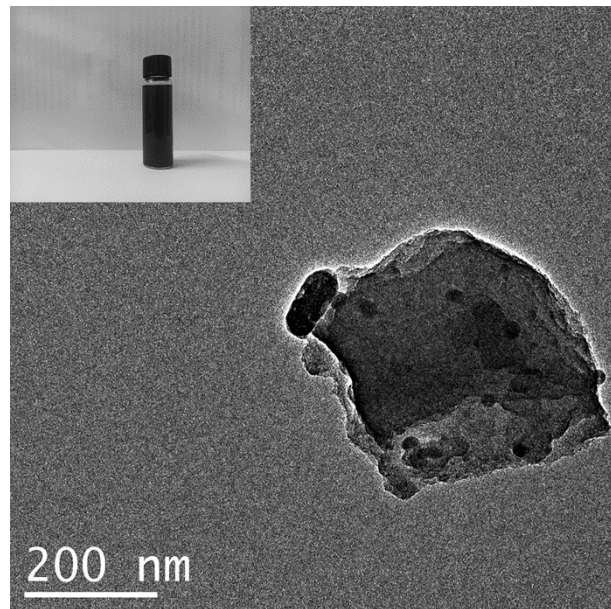


Fig. S3. TEM image of CTP after ultrasonication in hydrogen peroxide for 2 h. Inset is the optical image.

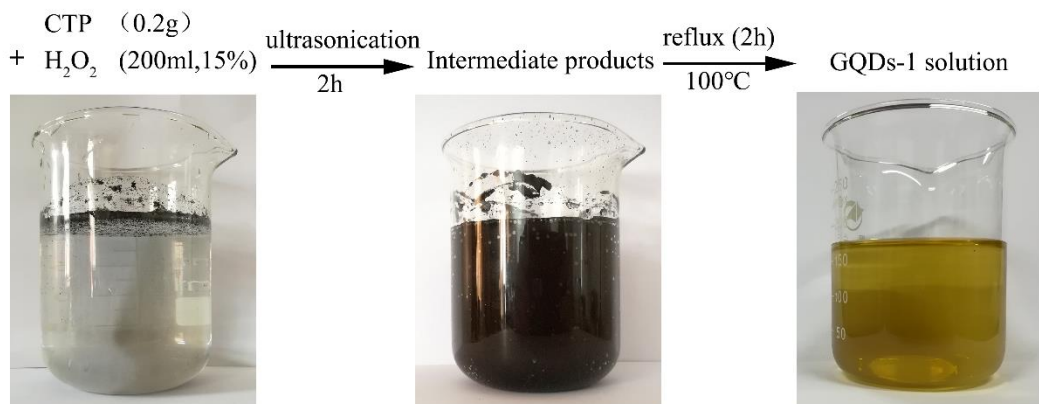


Fig. S4. Preparation procedure of GQDs-1.

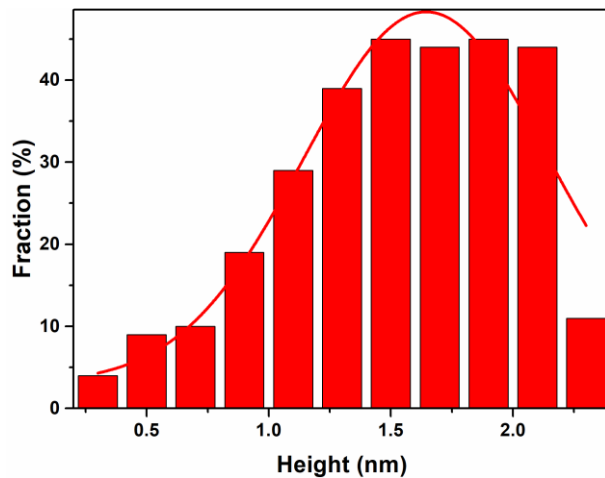


Fig. S5. The height distribution of the GQDs-1.

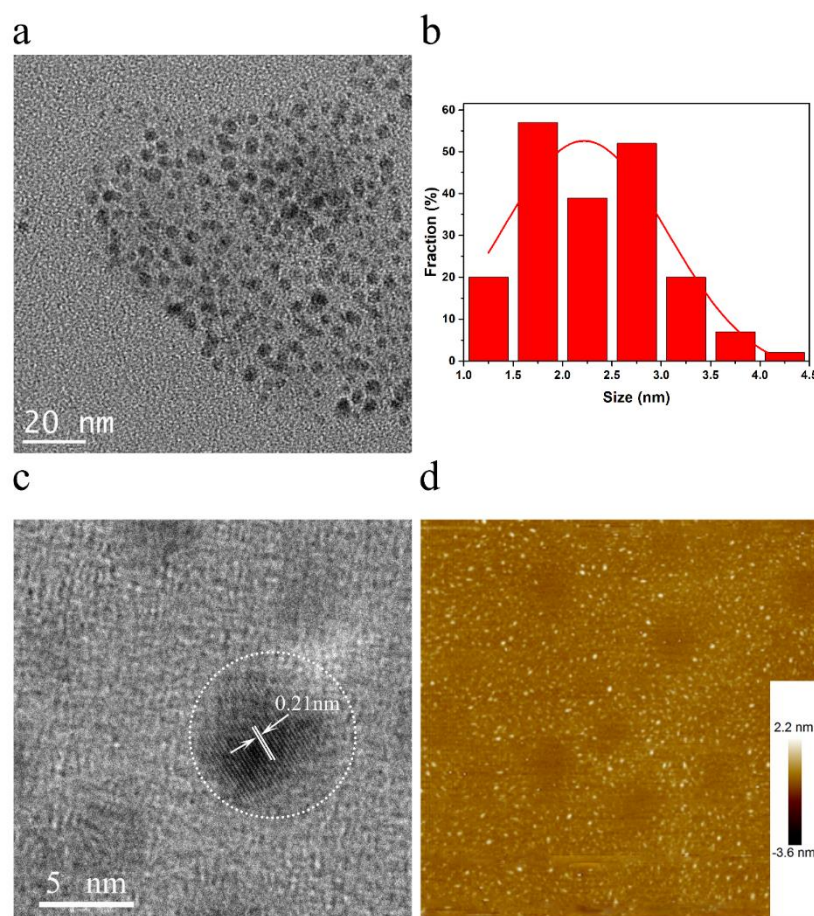


Fig. S6. Characterization of GQDs-2. (a) TEM image of GQDs-2 displaying a regular size and shape distribution. Scale bar, 20 nm. (b) The size distribution histogram of GQDs-2. (c) HRTEM image of representative GQDs-2 from a. (d) AFM image of GQDs-2.

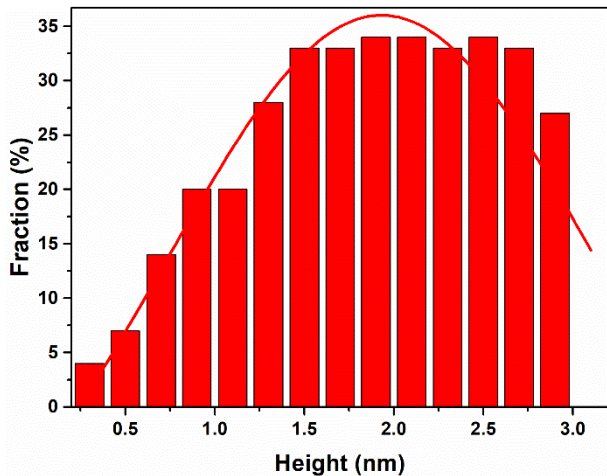


Fig. S7. The height distribution of the GQDs-2.

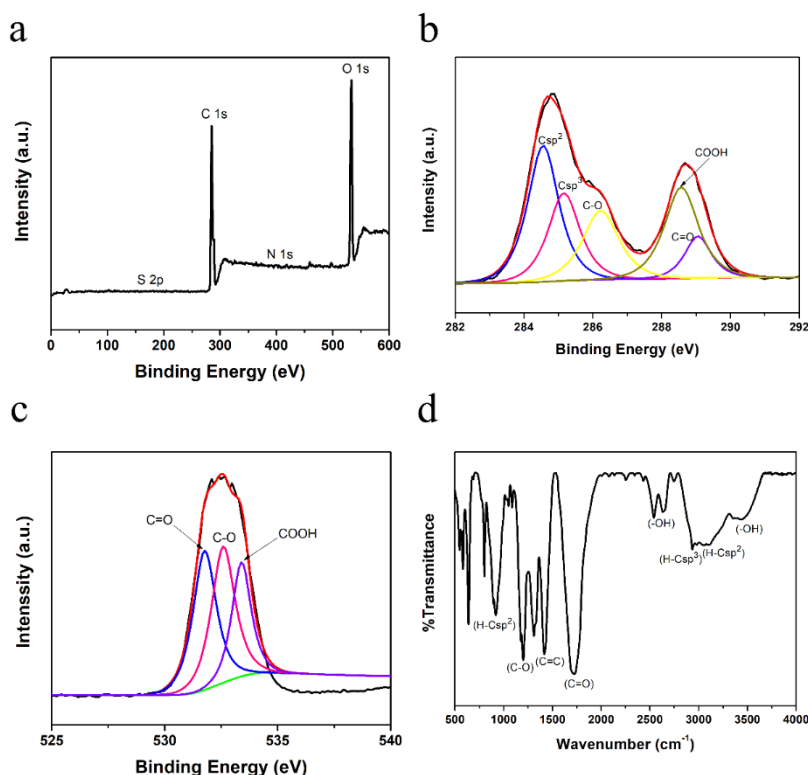


Fig. S8. Characterization of GQDs-2. (a) XPS survey of GQDs-2. (b) High-resolution C 1s XPS spectrum of GQDs-2. (c) The high-resolution O 1s XPS spectrum of GQDs-2. (d) ssFTIR spectrum of GQDs-2 showing different vibration modes as labeled.

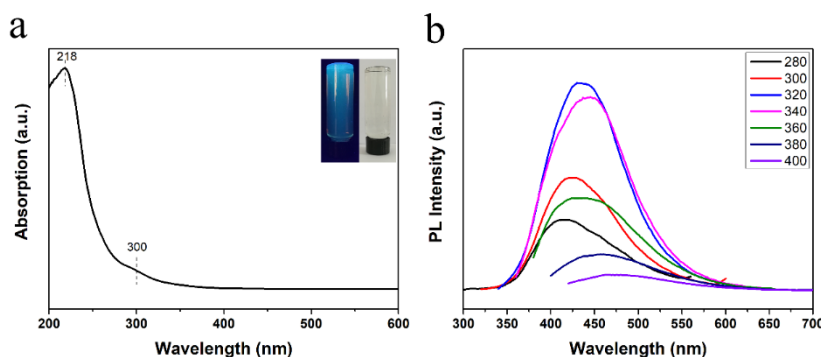


Fig. S9. Optical properties of the GQDs-2. (a) UV-Visible spectrum of the GQDs-2 dispersed in water. Inset of panel a: the left is a photograph of the corresponding GQDs-2 aqueous solution under UV light with 365 nm excitation; the right is a photograph of the corresponding GQDs-2 aqueous solution taken under visible light. (b) PL spectra of the GQDs-2 solution under different excitation wavelengths.

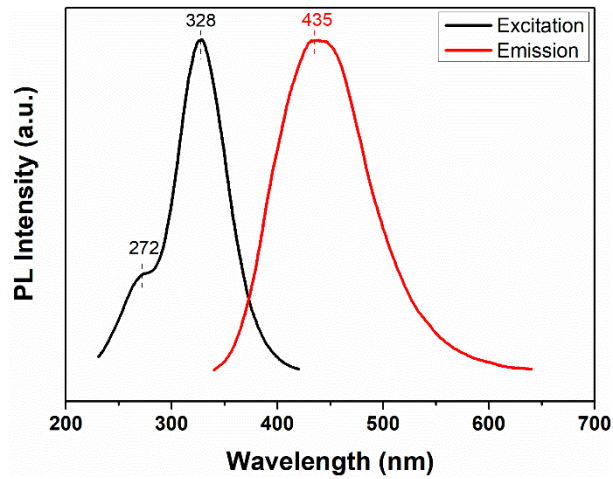


Fig. S10. PLE spectrum of GQDs-2 with the detection wavelength of 430 nm and PL spectrum excited at 328 nm.